1

Quantum Statistical Properties of the Light Emission from Quantum Dots in Microcavities

C. Gies, J. Wiersig, and F. Jahnke

Summary. A microscopic theory is presented and applied to describe luminescence and lasing from semiconductor quantum dots. Special emphasis is placed on the differences between quantum dots and atoms. We calculate the first- and second-order correlation functions to characterize the coherence properties and the photon statistics in current state-of-the-art microcavity lasers with high spontaneous emission coupling into the laser mode. To gain a deeper understanding of the derived laser theory and of the differences to atomic descriptions, a discussion of quantum-optical models is performed and placed in context to the semiconductor theory.

1.1 Introduction

Due to advances in growth and processing methods, together with ground breaking experimental achievements, the field of semiconductor quantum-dots is more rapidly evolving than ever. Part of this evolution is the need for appropriate theoretical models that encompass the experimental developments described in this book. The three-dimensional confinement of the carrier wave functions on a nanometer scale leads to a discrete part of the single-particle density of states. Semiconductor quantum dots (QDs) are therefore often viewed as "artificial atoms," and in the description of the emission properties of QDs models and approximations are frequently used that are well suited for atomic systems, but which have to be reconsidered when applied to semiconductor systems. In QDs, excitations can involve more than a single carrier. The resulting description of the interaction with the quantized light field is different when atomic systems with single-electron excitations and QDs with multiple excited carriers are compared, even though the elementary interaction processes remain the same. A central goal of our investigations is to reveal the influence of multiple excited carriers on the emission properties of QDs. In addition to the modification of the light-matter interaction itself, it is also well-known from various semiconductor systems that the interaction among the excited carriers leads to effects – many of them discussed throughout this book – that can modify or even dominate the emission properties and,

hence, should be included in semiconductor models. Pauli-blocking of states, the Coulomb interaction of excited carriers, their interaction with phonons, and a variety of resulting effects like energy renormalizations, contributions of new quasi-particles, or interaction-induced dephasing have been intensively studied also in QD systems. In atomic systems, interaction-induced effects are typically of minor importance and the single-particle excitations are subject to scattering and dephasing that is usually described via constant rates.

The placement of QDs in optical microcavities allows to tailor the coupling to the electromagnetic field, as is described in Chaps. 8 and 9. Very small mode volumes in combination with a high-quality mode enhance the spontaneous emission rate into that mode, a phenomenon known as Purcell effect [1–3]. While the effect can be employed for various applications like single-photon emitters (see, e.g., Chaps. 6 and 9) or LEDs with improved efficiency, we focus in the following on laser applications.

Due to the small size of the resonator, the high quality modes are usually spectrally well separated so that the QD ensemble can be considered to couple mainly to a single cavity mode. Still, a continuum of leaky modes provides dissipation channels via spontaneous emission. These modes, as well as the more weakly-coupled cavity modes, provide the non-lasing modes. A central parameter in lasers is the spontaneous emission coupling factor β that determines the fraction of the total spontaneous emission (SE) coupled into the laser mode:

$$\beta = \frac{\text{SE rate into laser mode}}{\text{total SE rate}} \,.$$

The Purcell effect can be used to enhance the spontaneous emission into the laser mode and to suppress spontaneous emission into non-lasing modes. For β approaching unity, the intensity jump in the input/output curve gradually disappears, which has lead to the discussion of a thresholdless laser [4,5]. Latest advances in the growth and design of semiconductor-QD microcavity lasers have now attained the regime of β-values close to unity experimentally [6–10]. To characterize these systems one needs to study the coherence properties of the emitted light and its statistical properties as function of the pump rate. Following Glauber, the quantum states of light can be characterized in terms of photon correlation functions [11]. Coherence properties are reflected by the correlation function of first order,

$$g^{(1)}(\tau) = \frac{\langle b^\dagger(t) b(t+\tau)\rangle}{\langle b^\dagger(t) b(t)\rangle} \,. \tag{1.1}$$

In the stationary regime this quantity depends only on the delay time τ but not on the time t. Its decay in τ is determined by the coherence time of the emitted light. Here $b^\dagger$ and b are the creation and annihilation operators for photons in the laser mode. Information about the statistical properties of the emitted light can be obtained from the correlation function of second order at zero delay time

$$g^{(2)}(\tau = 0) = \frac{\langle n^2 \rangle - \langle n \rangle}{\langle n \rangle^2} = \frac{\langle b^\dagger b^\dagger b b \rangle}{\langle b^\dagger b \rangle^2}, \tag{1.2}$$

where $n = b^\dagger b$ is the photon number operator for the laser mode. The function $g^{(2)}(\tau = 0)$ reflects the possibility of the correlated emission of two photons at the same time. For the characterization of the light field, this quantity is of central importance throughout this book. Note that in other chapters a and $a^\dagger$ are used for the photon operators, which is the common notation in quantum optics. Often discussed are the limiting cases of light emission from a thermal, coherent, and single-photon source. Thermal light is characterized by an enhanced probability that two photons are emitted at the same time (bunching), reflected in a value of $g^{(2)}(0) = 2$. For coherent light emission with Poisson statistics one finds $g^{(2)}(0) = 1$. An ideal single-photon emitter shows antibunching with $g^{(2)}(0) = 0$. The full photon statistics corresponding to these limiting cases is discussed in Chap. 6.

This first chapter is concerned with the emission properties of microcavity lasers with QDs as active material. The considered QD and atomic models are introduced in Sect. 1.2. In Sect. 1.3 we discuss several well-established quantum optical models, namely the rate equations, a master equation approach and the Liouville/von-Neumann equation. These models are placed in relation to each other and to the equation-of-motion approach that we use in Sects. 1.4 and 1.5 to develop a microscopic semiconductor model to describe the interaction of the QD emitters with the laser and non-lasing modes. This model allows us to access the statistical properties of the light emission, described in terms of the second-order photon correlation function (1.2). The calculation of first-order correlation function (1.1) and the coherence time is the topic of Sect. 1.6.

1.2 Quantum Dots and Atoms

In QDs a three-dimensional confinement of carriers leads to localized states both for conduction- and valence-band carriers, and discrete interband transition energies between these so-called shells. In the frequently used self-assembled QDs the discrete states appear energetically close to a quasi-continuum of delocalized states that corresponds to the two-dimensional motion of carriers in a wetting layer (WL). A sketch of the corresponding energy levels of conduction and valence band states in the vicinity of the optical band gap is shown in Fig. 1.1.

The finite height of the confinement potential restricts the number of confined shells. As discussed in Chap. 2 one can control the number of shells and their separation in energy by variation of the growth parameters. For self-assembled QDs one usually finds a strong confinement in growth direction and weaker confinement in the WL plane. Because of the strong confinement only the energetically lowest state is important for the motion in

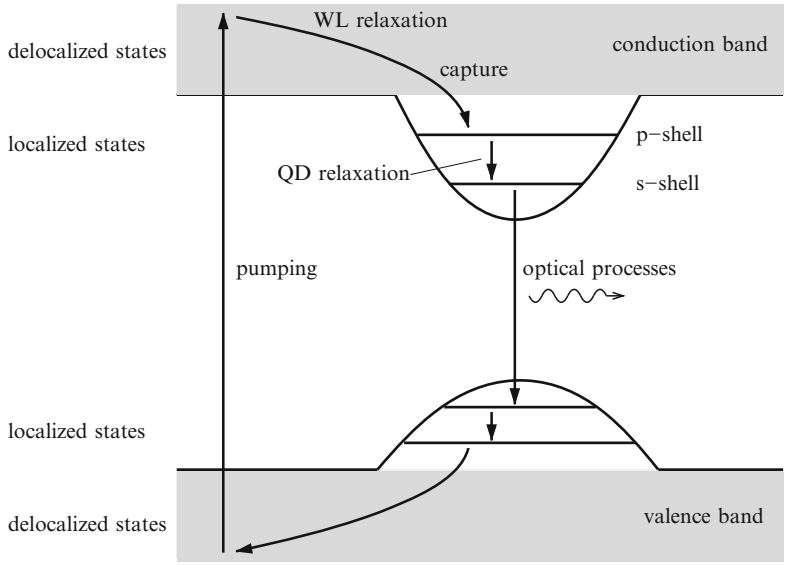

Fig. 1.1. Schematic representation of energy levels in a quantum dot (QD) with two shells for carriers in the conduction and valence band, respectively. The quasi-continuum of the wetting layer (WL) is shown as *shaded areas*

the growth direction, while for the in-plane problem one finds in general several bound states. Moreover, in the lens-shaped QDs the in-plane rotational symmetry leads to an angular-momentum degeneracy in addition to the spin degeneracy of the weakly confined states. In the following, we consider QDs where the confinement leads to two shells for conduction- and valence-band carriers. Then one *s*-shell and two *p*-shell states are available for each spin-subsystem. The unexcited state corresponds to filled valence-band states and empty conduction-band states.

To investigate the optical properties of QDs, the system may be off-resonantly excited by an optical pulse. The excitation creates carriers in the barrier-, WL-, or higher QD-states. Fast scattering (relaxation) into the lower QD states, as illustrated in Fig. 1.1, is facilitated by carrier–carrier and carrier–phonon interaction [12,13]. At low temperatures and at low to moderate carrier densities, the carriers populate solely the QD states. Then the WL states are mainly important for carrier-scattering processes if the excitation involves the quasi-continuum. In the following we are interested in the recombination dynamics due to carrier–photon interaction involving the localized QD states. We study a laser system based on QDs in optical microresonators, where we assume that the energetically lowest interband transition between the *s*-shells of the conduction and valence bands is dipole allowed and in resonance with the fundamental cavity mode.

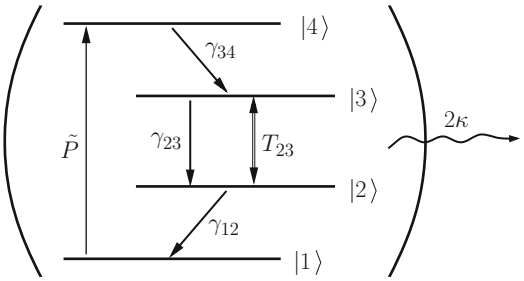

Fig. 1.2. Diagram of the atomic four-level laser system. With the pump rate $\tilde{P}$ an electron is excited from the ground state $|1\rangle$ into the pump level $|4\rangle$. The rates γ_{34} and γ_{12} determine the scattering into and from the laser levels $|2\rangle$ and $|3\rangle$, which are coupled to the laser mode via the transition amplitude T_{23}. Emission into non-lasing modes is described by the rate γ_{23}. The cavity mode is coupled to a reservoir of modes outside the cavity, giving rise to cavity losses 2κ

For the discussed QD system, it is tempting to exploit the similarities to an atomic four-level system displayed in Fig. 1.2.[1] The important difference to the semiconductor case is that the unexcited QD system contains filled valence-band states. Inevitably more than a single electron can be excited into the conduction-band states.

To obtain the closest possible analogy between the QD system of Fig. 1.1 and the atomic four-level system of Fig. 1.2, we assume that only two confined QD shells for electrons and holes, respectively, (denoted by s and p) are relevant and that the optical pump process is resonant with the p-shells.

The presence of more than one electron in the interacting discrete level system complicates the direct application of well-established models from quantum optics and requires their reformulation. At this point one might argue, that the elementary optical excitations are excitons, which consist of conduction-band electrons and the corresponding valence-band vacancies bound by the Coulomb interaction. However, the exciton operators obey bosonic commutators only in the absence of other carriers. While a formulation in a pure bosonic exciton picture clearly oversimplifies the problem, the inclusion of corrections is highly nontrivial and as such can be viewed as a reformulation of the fermionic electron–hole picture employed below.

[1] At this point we would like to add a general remark about the interpretation of the atomic model. The considered transitions take place between different configurations of the system, which may involve occupations of several states, again involving more than one carrier. However, in quantum-optical models transitions between these configurations are treated analogously to transitions between electronic states. Therefore, we speak of an atomic system with a single electron that can occupy any of the available levels, keeping in mind that while this is a simplified picture, formally the single-electron model is equivalent to the configuration picture.

To summarize this central point, the presence of multiple excited carriers and their mutual interaction is usually not an issue in atomic quantum optics, but it is of key importance in semiconductor optics. Other complications in the application of well established models in quantum optics to QD systems are of more practical nature and involve the applicability of approximations commonly applied to atomic systems. Examples are reabsorption of photons in connection with incomplete inversion of the laser transition, saturation effects, or interaction-induced dephasing.

In the following we start from standard models in quantum optics, that describe the interaction of the quantized light field with atomic systems characterized by "single-electron excitations" in the sense we have discussed above. These approaches are related in a second step to our semiconductor models that account for the excitation of multiple carriers and their interaction.

1.3 Light-Matter Interaction in Atomic Systems

1.3.1 Liouville/von-Neumann Equation

In quantum optics the most general approach to atom-photon interaction is to solve the Liouville/von-Neumann equation for the full density matrix ρ of the coupled carrier–photon system. From the density-matrix elements, arbitrary single-time expectation values can be obtained by calculating the trace. However, the full solution of the von-Neumann equation is only feasible for small systems (few atoms). Most familiar is the direct solution of the density-matrix equations for the Jaynes–Cummings Hamiltonian, that describes the interaction of a two-level system with the quantized light field. This model can be extended to a one-atom laser while still permitting a direct solution of the density-matrix equations, as discussed in [14]. For this purpose, the two-level system for the resonant optical interaction with the laser mode is augmented by two additional levels in order to facilitate the pump process and a rapid depletion of the lower laser level, as shown in Fig. 1.2. The model still contains a single electron that, if in the ground state $|1\rangle$, can be excited into the pump level $|4\rangle$. Transition processes between the levels and the corresponding dephasing of the off-diagonal density matrix elements are introduced by coupling the atom to reservoirs. The interaction with these reservoirs is treated in the so-called Born–Markov approximation [15] and is contained in the resulting transition rates $\tilde{P}$ and γ_{ij} indicated in Fig. 1.2. Of particular importance are fast transitions into the upper laser level $|3\rangle$ at the rate γ_{34} and rapid processes emptying the lower laser level $|2\rangle$ at the rate γ_{12}. For the transitions between the laser levels $|3\rangle$ and $|2\rangle$, the spontaneous emission into non-lasing modes, described by the rate γ_{23}, competes with the coupling to the laser mode via the transition amplitude T_{23}. By coupling also the laser mode to a reservoir as discussed above, cavity losses with a rate 2κ are introduced.

The time evolution of the full density matrix ρ can be obtained from its commutator with the Jaynes–Cummings Hamiltonian H_{JC} and the dissipative and pump processes are described by Lindblad terms $L\rho$ (that account for the above discussed coupling to the reservoirs [15]) according to

$$\frac{\mathrm{d}}{\mathrm{d}t}\,\rho = -\frac{i}{\hbar}[H_{\mathrm{JC}}, \rho] + L\rho\,. \tag{1.3}$$

The model can be extended to N atoms interacting with the quantized light field. Via the off-diagonal density-matrix elements coupling between different atoms is included. This coupling is connected to superradiance/ superfluorescence. A direct numerical solution or the application of quantum Monte-Carlo techniques, however, is presently restricted to a small numbers of atoms.

1.3.2 Master Equations

A considerable simplification of the theory is possible if one can formulate closed equations for the diagonal density matrix elements, which represent probabilities. One can deduce such a treatment from the Liouville/von-Neumann equation by adiabatically eliminating the off-diagonal density matrix elements. In the adiabatic regime, the dephasing is sufficiently fast to dominate over the dynamics, so that the off-diagonal elements simply follow without delay their sources (incoherent regime). Furthermore, the contributions of the cavity losses to the dephasing of the off-diagonal density matrix elements need to be small [14].

An additional, commonly used approximation consists in neglecting the reabsorption of photons from the cavity mode. When the state $|2\rangle$ in Fig. 1.2 is rapidly depopulated via the scattering process γ_{12}, the reabsorption process is suppressed and the laser transition benefits from maximal inversion for a given pump rate $\tilde{P}$. In this case, the recombination rate is determined by the probability of finding the electron in the upper laser level together with a given number of photons in the cavity mode. A system containing many atoms can then be characterized by the probabilities $p_{n,N}$ of states with N excited atoms and n photons in the laser mode.

Deriving the master equation for $p_{n,N}$ from the Liouville/von-Neumann equation the way we have discussed it is a stringent approach. Often a phenomenological approach based on intuitive arguments is taken that leads to the same results. By considering all relevant processes that can act on a given state of the system, a birth/death model can be formulated where phenomenological transition rates are introduced. This is illustrated in Fig. 1.3 where λ is the cavity loss rate, P the pump rate and β is the spontaneous emission coupling factor. The arrows describe processes that can act on the state $p_{n,N}$, see the figure caption. As an example we consider the spontaneous emission into non-lasing modes, indicated as dashed lines in the vertical direction since

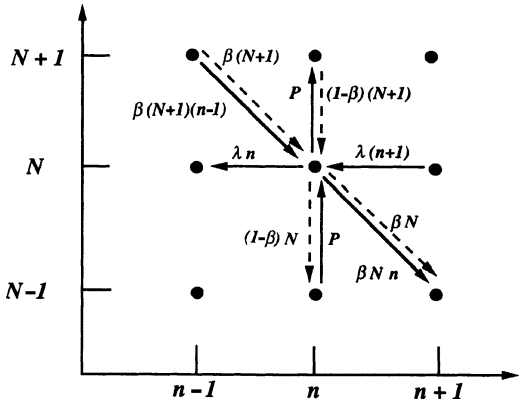

Fig. 1.3. Schematic representation of the relevant processes in the birth/death model. On the *vertical axis* the number of excited emitters N is shown, on the *horizontal axis* the number of photons n in the cavity. In the diagram, each *dot* stands for a matrix element of the diagonal density matrix $\rho_{n,N}$ and represents a state with the corresponding number of excited atoms and photons. Processes acting on a state with probability $\rho_{n,N}$ are: cavity losses, keeping the number of excited atoms unaltered and thus represented as *horizontal line*; pump process, keeping the number of photons unaltered and thus represented as *vertical line*; spontaneous and stimulated emission, where the number of excited emitters is reduced and the number of photons in increased, thus represented as *diagonal lines*. The rates related to each process are noted with the *arrows*. Figure reprinted with permission from P.R. Rice and H.J. Carmichael [5], copyright 1994 by the American Physical Society

the number of photons in the cavity remains unaltered by this process. The contribution to the equation of motion is read off the schematic as

$$\frac{\mathrm{d}}{\mathrm{d}t}\, p_{n,N}\Big|_{\mathrm{nl}} = -\frac{(1-\beta)}{\tau_{\mathrm{sp}}}\,\left[N p_{n,N} - (N+1) p_{n,N+1}\right]. \tag{1.4}$$

The prefactor $(1-\beta)/\tau_{\mathrm{sp}}$ describes the rate of spontaneous emission into non-lasing modes, assuring that there is no emission at all into these modes in the case $\beta = 1$. There are two possibilities involving a state with N excited emitters, either a decay ("death") of the very same state (after emission a state with $N-1$ excited emitters is left), or its "birth" by the decay of a state with $N+1$ excited emitters. The full master equation with all contributions displayed in Fig. 1.3 can be found in [5].

Despite the involved approximations when going to the master equation from the Liouville/von-Neumann equation, the possibility remains to calculate the photon statistics $p_n = \sum_N p_{n,N}$, and hence $\langle n\rangle, \langle n^2\rangle, \ldots$, as well as arbitrary photon correlation functions, where all operators have equal time arguments.

1.3.3 Rate Equations

From the Liouville/von-Neumann or the master equation, it is also possible to derive equations of motion for expectation values like the mean number of excited atoms and photons in the laser mode, $\langle N \rangle$ and $\langle n \rangle$, respectively. These equations couple to higher-order expectation values and as such form an infinite hierarchy of equations. The truncation of this hierarchy requires factorization approximations.

In the most simple form of such a truncation correlations between atoms and photons are completely neglected, i.e., $\langle nN \rangle = \langle n \rangle \langle N \rangle$. Since these terms appear only in the contributions representing stimulated emission, the treatment of these processes then corresponds to a semi-classical picture. Spontaneous emission, on the other hand, is not influenced by this approximation. Then one obtains from the equations of motion for $\langle n \rangle \equiv n$ and $\langle N \rangle \equiv N$ the well-established laser rate equations

$$\frac{\mathrm{d}}{\mathrm{d}t} n = -2\kappa n + \frac{\beta}{\tau_{\mathrm{sp}}} \left[1 + n\right] N, \tag{1.5}$$

$$\frac{\mathrm{d}}{\mathrm{d}t} N = -\frac{\beta}{\tau_{\mathrm{sp}}} nN - \frac{1}{\tau_{\mathrm{sp}}} N + \tilde{P}. \tag{1.6}$$

The photon population is determined by the interplay of the cavity loss rate 2κ and the photon generation due to spontaneous processes $\propto N$ and stimulated processes $\propto nN$. The dynamics of the number of excited emitters N follows from the interplay of the carrier recombination and the pump rate $\tilde{P}$. The former comprises stimulated emission into the laser mode $\propto \beta/\tau_{\mathrm{sp}} = 1/\tau_{\mathrm{l}}$, and spontaneous emission $\propto 1/\tau_{\mathrm{sp}}$ into all available modes. For a detailed discussion of the laser rate equations, see, e.g., [5, 16].

In the following we discuss the stationary solution of the rate equations for a constant pump rate $\tilde{P}$. Results for the input/output curves and various values of the β-factor are shown in Fig. 1.4. We choose parameters that are typical for present microcavity lasers: $\tau_{\mathrm{sp}} = 50\,\mathrm{ps}$ and $\kappa = 20\,\mu\mathrm{eV}$. The corresponding cavity lifetime is about 17 ps, yielding a Q-factor of roughly $30,000$. At the laser threshold that differentiates the regimes of dominant spontaneous and stimulated emission, the photon number exhibits a jump $\propto \beta^{-1}$. In the limit $\beta = 1$ this kink in the input/output curve disappears and the threshold is no longer well defined in this simple picture. Note that the photon statistics obtained from the master equation provides additional information about a possible transition from thermal to coherent light emission. The discussed behavior of the jump in Fig. 1.4 is commonly used to estimate the β-factor from measurements.

The customary form of the master equation and the rate equations have in common that saturation effects do not appear. The reason lies in negligence of reabsorption processes and in the fact that the total number of available

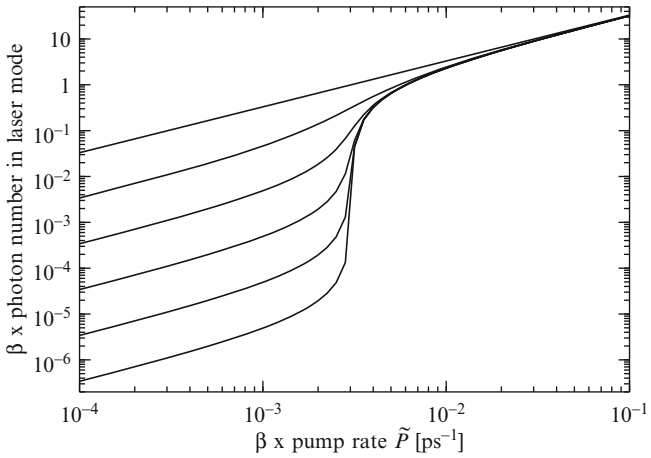

Fig. 1.4. Results from the laser rate equations (1.5) and (1.6) for $\beta = 1$ to 10^{-5} from *top* to *bottom*

atoms is not limited. This is important for the comparison to semiconductor-QD systems, where reabsorption and saturation effects can strongly modify the input/output curves.

It is by no means necessary to truncate the equations of motion at the simplest possible level that, as we have just shown, leads to the rate equations. The truncation can be performed on a higher level in the hierarchy. For the additional terms separate equations of motion have to be formulated. This way, for example, it is possible to obtain insight into the statistical properties of the light field, represented by the photon–photon correlations $\langle n^2 \rangle$, via the equation-of-motion approach in an analogous fashion to the rate equations. A critical issue remains with the inclusion of multiple excited carriers and their interaction. As discussed in Sect. 1.2, several carriers can be excited in semiconductor QDs.

Before the microscopic semiconductor theory is presented in Sect. 1.5, we give an illustrative explanation of how the emission properties are directly influenced by this difference to atomic systems.

1.4 Multiple Excited Carriers in Semiconductor QDs

1.4.1 Electron–Hole Picture

The QD level scheme of Fig. 1.1 with optical pumping into the *p*-states, fast relaxation of carriers from *p* to *s*-states, and resonant interaction with the laser mode via the *s*-states is translated into the electron–hole-picture in Fig. 1.5. Since for the unexcited system the valence-band states are filled (holes are absent) a richer set of possible states can be realized in comparison to the

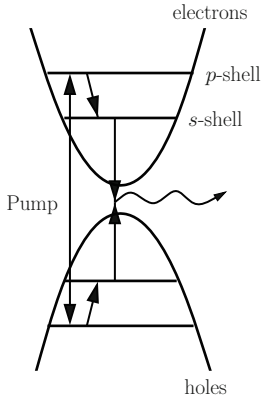

Fig. 1.5. QD laser model with carrier generation in the *p*-shells and the laser transition between the *s*-shells of electrons (*top*) and holes (*bottom*)

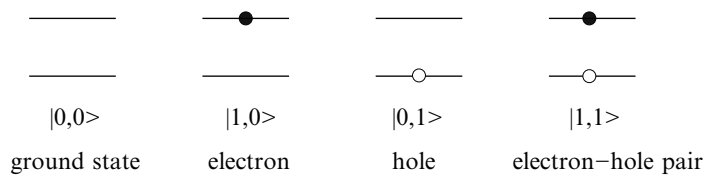

Fig. 1.6. Schematic level diagram of possible electron and hole occupations for the *s*-shell of a quantum dot. The photonic part of the states is of no relevance for the discussion in the text and, therefore, not explicitly shown

single-electron system in Fig. 1.2. For the *s*-states, the possible configurations are displayed in Fig. 1.6. In the second (third) configuration recombination is not possible since the hole (electron) is missing.

In the one-electron systems discussed in Sect. 1.3, the second configuration where electrons are present in both laser levels is impossible. In the third configuration no electrons are present in the *s*-shell at all. In the description based on the full density matrix in Sect. 1.3.1 this is possible if the carrier resides in a *p*-shell state (corresponding either to the state $|1\rangle$ or $|4\rangle$ in the scheme in Fig. 1.2). However, when the scattering processes γ_{12} and γ_{34} in Fig. 1.2 are sufficiently fast, this configuration is unlikely and, correspondingly, left out in the models discussed in Sects. 1.3.2 and 1.3.3.

1.4.2 Theory of QD Recombination

For the following discussion we consider the coupling of carriers in one spin subsystem to the corresponding circular polarization component of the light field. The four *s*-shell states are denoted by $|n_\mathrm{e}, n_\mathrm{h}\rangle$ with $n_\mathrm{e} = 0, 1$ and $n_\mathrm{h} = 0, 1$. For the calculation of the recombination dynamics we focus on

the incoherent regime. Then the elements of the density matrix traced over the photonic and p-shell states are given by

$$\rho = P_{00}|0,0\rangle\langle 0,0| + P_{10}|1,0\rangle\langle 1,0| + P_{01}|0,1\rangle\langle 0,1| + P_{11}|1,1\rangle\langle 1,1| \tag{1.7}$$

with the probabilities $0 \leq P_{ij} \leq 1$ and the normalization condition

$$\mathrm{tr}(\rho) = \sum_{i,j=0}^{1} P_{ij} = 1. \tag{1.8}$$

In the formalism of second quantization the states $|n_\mathrm{e}, n_\mathrm{h}\rangle$ are related to each other by creation and annihilation operators. The fermionic operator e ($e^\dagger$) annihilates (creates) an electron. The corresponding operators for holes are h and $h^\dagger$. For instance, applying the creation operator $e^\dagger$ to the ground state $|0,0\rangle$ yields the one-electron state $|1,0\rangle$. In the same way, the creation operator $h^\dagger$ turns the ground state into the one-hole state $|0,1\rangle$. The formalism of second quantization allows to describe many-particle effects in an elegant way. Relevant quantities can be expressed as expectation values of products of creation and annihilation operators. For example, the luminescence is determined by the dynamics of the photon number $\langle b^\dagger b\rangle$, where the bosonic operator b ($b^\dagger$) annihilates (creates) a photon in a given optical mode. Other relevant quantities are the occupations of electrons $f^\mathrm{e} = \langle e^\dagger e\rangle$ and holes $f^\mathrm{h} = \langle h^\dagger h\rangle$. The changes of the photon number $\langle b^\dagger b\rangle$ and of the s-shell occupation probabilities $\langle e^\dagger e\rangle$, $\langle h^\dagger h\rangle$ are determined by mixed expectation values $\langle b^\dagger he\rangle$ as discussed in detail in Sect. 1.5. The general form of these equations allows to describe not only the interplay of the different configurations shown in Fig. 1.6, but also the inclusion of many-body Coulomb effects on various levels of refinement.

In the following discussion we are only interested in the spontaneous recombination processes. For the purpose of uncovering essential differences between the single-electron atomic system and the many-electron QD system, we neglect only for the following discussion the effects of Coulomb interaction and use an adiabatic elimination of mixed expectation values $\langle b^\dagger he\rangle$ that represent interband transition amplitudes. With these approximations the decay of carrier population is determined by

$$\frac{\mathrm{d}}{\mathrm{d}t} f^{(e,h)}\Big|_\mathrm{spont} = -\frac{\langle e^\dagger e\; h^\dagger h\rangle}{\tau}, \tag{1.9}$$

where $1/\tau$ is the rate of spontaneous emission. Even though formula (1.9) is based on a considerable simplification in comparison to the general theory, it reveals the basic difference between QDs and atomic systems with single excited carriers. To see this, we express $\langle e^\dagger e\; h^\dagger h\rangle$ in terms of the four basis states illustrated in Fig. 1.6. We first note that $e|0,n_\mathrm{h}\rangle = 0$ as one cannot

remove an electron from a state that does not contain one. Equally, $h|n_\mathrm{e}, 0\rangle = 0$. From this follows immediately $e^\dagger e\ h^\dagger h|n_\mathrm{e}, n_\mathrm{h}\rangle \neq 0$ only if $n_\mathrm{e} = n_\mathrm{h} = 1$. Using this relation we find

$$\langle e^\dagger e\ h^\dagger h\rangle = \mathrm{tr}(\rho\, e^\dagger e\ h^\dagger h) = P_{11}. \tag{1.10}$$

The intuitive interpretation is, that the decay of carrier population described in (1.9) is proportional to the probability P_{11} of finding an electron–hole pair, since only in state $|1,1\rangle$ the electron and the hole can recombine via emission of a photon.

For the semiconductor system with multiple excited carriers, the probability of observing an electron–hole pair is in general different from the probability of finding an electron (or a hole). This can be seen by rewriting the occupation probability of electrons as

$$f^\mathrm{e} = \langle e^\dagger e\rangle = \mathrm{tr}(\rho\, e^\dagger e) = P_{10} + P_{11}. \tag{1.11}$$

Along the same lines one obtains for the holes

$$f^\mathrm{h} = P_{01} + P_{11}. \tag{1.12}$$

Comparing (1.11) or (1.12) with (1.10) reveals that the probability of finding an electron–hole pair is smaller than or equal to the probability of finding an electron or a hole, and equal to only if $P_{10} = P_{01} = 0$. In this particular case we can write (1.9) as

$$\frac{\mathrm{d}}{\mathrm{d}t} f^{(e,h)}\Big|_\mathrm{spont} = -\frac{f^{(e,h)}}{\tau}. \tag{1.13}$$

Assuming that no other mechanism contributes to the change of the population, it follows an exponential decay with rate $1/\tau$ for the population, which also carries over to the photoluminescence [17]. The conditions $P_{10} = P_{01} = 0$ reduce the four-state system for the electron and hole to a *two-state system* for the electron–hole pair with basis states $|0,0\rangle$ and $|1,1\rangle$. This situation corresponds to *fully correlated carriers*: the absence (presence) of an electron implies the absence (presence) of a hole and vice versa.

In the opposite limiting case of *uncorrelated carriers*, the joint probabilities P_{ij} factorize into the probabilities P_i^e for the electron and P_j^h for the hole, i.e., $P_{ij} = P_i^\mathrm{e} P_j^\mathrm{h}$. Accordingly the two-particle quantity $\langle e^\dagger e\ h^\dagger h\rangle$ factorizes into one-particle quantities

$$\langle e^\dagger e\ h^\dagger h\rangle_\mathrm{HF} = \langle e^\dagger e\rangle\langle h^\dagger h\rangle = f^\mathrm{e} f^\mathrm{h}. \tag{1.14}$$

This is the Hartree–Fock (HF) factorization. Note that polarization-like averages of the form $\langle e^\dagger h^\dagger\rangle$ vanish in the incoherent regime. The product $f^\mathrm{e} f^\mathrm{h}$ is the uncorrelated electron–hole population. Equations (1.10)–(1.12) show that

one can interpret (1.14) as the factorization of the probability of finding an electron–hole pair into the product of the individual probabilities of finding an electron and a hole.

Replacing $\langle e^\dagger e\, h^\dagger h\rangle$ in (1.9) by its HF-factorization (1.14) yields

$$\frac{\mathrm{d}}{\mathrm{d}t} f^{(e,h)}\Big|_{\text{spont}} = -\frac{f^{\mathrm{e}} f^{\mathrm{h}}}{\tau}. \tag{1.15}$$

From (1.15) it is obvious that the decay of the population f^{e} is non-exponential, unless f^{h} is held constant by some mechanism, like background doping. Furthermore, the decay rate depends on the carrier density and is higher for larger population.

In realistic situations the carriers in a semiconductor QD are neither fully correlated nor uncorrelated. To quantify the deviation from the discussed limiting cases, the correlation must explicitly be calculated.

The electron–hole correlation is defined as

$$\delta\langle e^\dagger e\, h^\dagger h\rangle = \langle e^\dagger e\, h^\dagger h\rangle - \langle e^\dagger e\, h^\dagger h\rangle_{\mathrm{HF}} = \langle e^\dagger e\, h^\dagger h\rangle - \langle e^\dagger e\rangle\langle h^\dagger h\rangle. \tag{1.16}$$

The relation to classical correlation functions can be seen more clearly in the following representation

$$\delta\langle e^\dagger e\, h^\dagger h\rangle = \langle \big(e^\dagger e - \langle e^\dagger e\rangle\big)\ \big(h^\dagger h - \langle h^\dagger h\rangle\big)\rangle. \tag{1.17}$$

While a variance like $\langle \big(e^\dagger e - \langle e^\dagger e\rangle\big)^2\rangle$ quantifies the fluctuations around the expectation value of a single quantity, the correlation function (1.17) is a covariance that quantifies correlated fluctuations of two different quantities. It can have positive and negative contributions depending on the relative sign of the two brackets in (1.17). A positive correlation function here means that on average the fluctuations of the electron and hole number around their respective expectation values have the same sign. In the case of a negative correlation function, the fluctuations have mostly opposite signs. We can identify the sources of positive and negative correlations in terms of the basis states $|n_{\mathrm{e}}, n_{\mathrm{h}}\rangle$ using the normalization condition (1.8)

$$\delta\langle e^\dagger e\, h^\dagger h\rangle = \sum_{n_{\mathrm{e}},n_{\mathrm{h}}=0}^{1} P_{n_{\mathrm{e}},n_{\mathrm{h}}}(n_{\mathrm{e}} - f^{\mathrm{e}})(n_{\mathrm{h}} - f^{\mathrm{h}}) = P_{00}P_{11} - P_{10}P_{01}. \tag{1.18}$$

The contribution from P_{00} and P_{11} enters with positive sign: if an electron is absent (present) the hole is absent (present). In contrast, the contribution from P_{10} and P_{01} enters with negative sign: if an electron is present (absent) the hole is absent (present). In other words, positive $\delta\langle e^\dagger e\, h^\dagger h\rangle$ implies that if we detect an electron then it is likely to find also a hole. Negative $\delta\langle e^\dagger e\, h^\dagger h\rangle$ implies that if we detect an electron then it is unlikely to find a hole. Vanishing correlation

$\delta\langle e^\dagger e\ h^\dagger h\rangle$ means that the two events of detecting an electron and detecting a hole are uncorrelated. In this particular case, the HF factorization (1.14) is exact.

1.4.3 QD Luminescence Dynamics

The fundamental behavior of carrier and luminescence dynamics can be visualized by considering a doped and an undoped system of semiconductor QDs. Details of this work can be found in [18]. In the doped case we choose the dopant density such that there is an average occupation of a single electron or hole per dot.

Figure 1.7 shows the time-resolved photoluminescence after excitation into the p-shell. The system is pumped with an equal electron and hole density of $N_\mathrm{e} = N_\mathrm{h} = 0.35N$ for a QD density of $N = 10^{10}\,\mathrm{cm}^{-2}$. In the doped case we assume on average one additional electron per QD, i.e., $N_\mathrm{e} = N_\mathrm{h} + N$ with again $N_\mathrm{h} = 0.35N$. Apart from this difference in the initial conditions both curves are calculated with exactly the same parameters. For the two different cases we see the following: In the situation of undoped QDs, we observe a non-exponential decay in agreement with our discussion. Again we would like to stress that the non-exponential decay cannot be predicted from an atomic theory. In contrast, the doped QDs show an exponential decay, which is faster by about a factor of two compared to the undoped case. This is due to the fact that the temporal change of the electron population relative to the doping level remains small. According to (1.15), a constant electron population f_ν^e leads to an exponential decay of the hole population f_ν^h, and, hence, of the photoluminescence intensity. This example nicely demonstrates the peculiarities of QD systems if thought of as "artificial atoms."

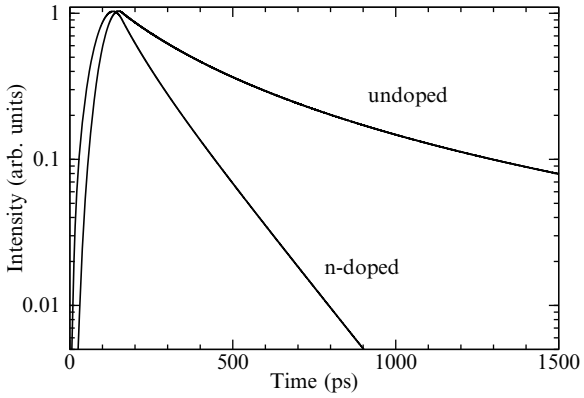

Fig. 1.7. Time-resolved photoluminescence for doped and undoped QDs excited into the p-shell

1.5 Quantum-Dot Microcavity Lasers

1.5.1 Semiconductor Theory

Our starting point is a Hamiltonian that contains the free carrier spectrum and the free electromagnetic field, as well as the light-matter interaction and Coulomb effects. For details we refer to [19]. The fermionic operators c_ν ($c_\nu^\dagger$) annihilate (create) electrons in the one-particle states $|\nu\rangle$ of energy ε_ν^c. The corresponding operators and single-particle energies for valence-band electrons are v_ν ($v_\nu^\dagger$) and ε_ν^v, respectively. The Bose operators b_ξ and $b_\xi^\dagger$ are the equivalents for photons in the mode ξ. We use the fact that polarization-like averages of the form $\langle v_\nu^\dagger c_\nu\rangle$ vanish due to the incoherent carrier generation, and so does the expectation value of the photon operators, $\langle b_\xi\rangle = 0$. Operator averages are obtained by means of the equation-of-motion technique and the cluster expansion method is used to truncate the inherent problem of an infinite number of coupled equations.

Cluster Expansion

The equation of motion of an average of N operators couples to $N+2$ operator averages due to the Coulomb and light-matter interactions. This hierarchy of equations must be truncated in an unambiguous way. One useful approach is the cluster expansion method [20]. As in (1.16), one schematically decomposes a four-operator average into

$$\langle a^\dagger a^\dagger a a\rangle = \langle a^\dagger a\rangle\langle a^\dagger a\rangle + \delta\langle a^\dagger a^\dagger a a\rangle, \tag{1.19}$$

denoting the fermionic carrier operators c, v by a. The first term on the right-hand side is called singlet contribution as it contains only single-particle quantities. For a four-operator average, the singlet factorization corresponds to the Hartree–Fock approximation. The second term is the correlation, which is a doublet contribution. It describes genuine two-particle effects.

The equation of motion for the four-operator (two-particle) correlation couples to averages of six operators, which are schematically factorized according to

$$\langle a^\dagger a^\dagger a^\dagger a a a\rangle = \langle a^\dagger a\rangle\langle a^\dagger a\rangle\langle a^\dagger a\rangle + \langle a^\dagger a\rangle\,\delta\langle a^\dagger a^\dagger a a\rangle + \delta\langle a^\dagger a^\dagger a^\dagger a a a\rangle \tag{1.20}$$

into singlet, singlet-doublet and triplet contributions. Note that all possible combinations of averages and correlations must be taken, meaning that each of the first two terms on the right-hand side may represent several terms of the same order. The triplet contribution, the last term in (1.20), contains only genuine three-particle effects. In this formulation, the truncation of the hierarchy can be consistently performed on all correlation functions of a certain order N, meaning that all correlations involving up to $N-1$ particles are included.

The same scheme can be applied to mixed averages of fermionic carrier and bosonic photon operators. Considering interband transitions, it must be borne in mind that the excitation of one electron is described as the destruction of a valence band carrier and the creation of a conduction band carrier. For the corresponding interaction processes, a photon operator is connected to *two* carrier operators [21, 22].

As an example for possible factorizations, we consider the factorization of the operator average $\langle b^\dagger b b^\dagger v^\dagger c\rangle$ into two doublets, which is obtained after normal order is established, i.e.,

$$\begin{aligned}\langle b^\dagger b b^\dagger v^\dagger c\rangle\Big|_{\text{doublet}} &= \left\{\langle b^\dagger v^\dagger c\rangle + \langle b^\dagger b^\dagger b v^\dagger c\rangle\right\}_{\text{doublet}} \\ &= \delta\langle b^\dagger v^\dagger c\rangle\left[1+2\delta\langle b^\dagger b\rangle\right].\end{aligned} \tag{1.21}$$

In the equation-of-motion approach we pursue, the hierarchy of coupled equations must be extended to the so-called quadruplet-level in order to calculate the photon statistics. This can be seen by expressing (1.2) in terms of correlation functions, $\delta\langle b^\dagger b^\dagger b b\rangle = \langle b^\dagger b^\dagger b b\rangle - 2\langle b^\dagger b\rangle^2$, where the factor of two arises from the two possible realizations for this factorization. Since $\langle b\rangle = \langle b^\dagger\rangle = 0$ for a system without coherent excitation only a factorization into doublets is possible. Then the autocorrelation function can be written in terms of the quadruplet correlation function $\delta\langle b^\dagger b^\dagger b b\rangle$:

$$g^{(2)}(\tau=0) = 2 + \frac{\delta\langle b^\dagger b^\dagger b b\rangle}{\langle b^\dagger b\rangle^2}. \tag{1.22}$$

In experiments $g^{(2)}(\tau)$ can be determined, e.g., in a Hanbury–Brown Twiss setup, which is discussed in Chaps. 6 and 11.

Equations of Motion

For the dynamical evolution of the photon number $\langle b_\xi^\dagger b_\xi\rangle$ in the mode ξ and the carrier populations $f_\nu^{\mathrm{e}} = \langle c_\nu^\dagger c_\nu\rangle$, $f_\nu^{\mathrm{h}} = 1 - \langle v_\nu^\dagger v_\nu\rangle$, the contribution of the light matter (LM) interaction in the Heisenberg equations of motion leads to

$$\left(\hbar\frac{\mathrm{d}}{\mathrm{d}t} + 2\kappa_\xi\right)\langle b_\xi^\dagger b_\xi\rangle = \quad 2\,\mathrm{Re}\sum_{\nu'}|g_\xi|^2\,\langle b_\xi^\dagger v_{\nu'}^\dagger c_{\nu'}\rangle, \tag{1.23}$$

$$\hbar\frac{\mathrm{d}}{\mathrm{d}t} f_\nu^{\mathrm{e,h}}\Big|_{\mathrm{LM}} = -2\,\mathrm{Re}\sum_{\xi}|g_\xi|^2\,\langle b_\xi^\dagger v_\nu^\dagger c_\nu\rangle. \tag{1.24}$$

Note that we have scaled $\langle b_\xi^\dagger v_\nu^\dagger c_\nu\rangle \to g_\xi\,\langle b_\xi^\dagger v_\nu^\dagger c_\nu\rangle$ with the light-matter coupling strength g_ξ to have its modulus appear in the above equations. The notation is to be understood as follows: A new quantity $\widetilde{\langle b_\xi^\dagger v_\nu^\dagger c_\nu\rangle} = \langle b_\xi^\dagger v_\nu^\dagger c_\nu\rangle/g_\xi$ is

used and the tilde is dropped in the following. In (1.23) we have introduced the loss rate $2\kappa_\xi/\hbar$. The mode index labels cavity as well as leaky modes. For the laser mode ξ_l, the loss rate is directly connected its Q-factor, $Q = \hbar\omega_{\xi_\mathrm{l}}/2\kappa_{\xi_\mathrm{l}}$. The dynamics of the photon number in a given mode is determined by the photon-assisted polarization $\langle b_\xi^\dagger v_\nu^\dagger c_\nu\rangle$ that describes the expectation value for a correlated event, where a photon in the mode ξ is created in connection with an interband transition of an electron from the conduction to the valence band. The sum over ν involves all possible interband transitions from various QDs, i.e., $\nu = \{\mu, \mathbf{R}\}$ with μ being the shell index and $\mathbf{R}$ the QD position. The dynamics of the carrier population in (1.24) is governed by contributions of photon-assisted polarizations from all possible modes (both lasing and non-lasing modes).

The time evolution of the photon-assisted polarization is given by

$$\begin{aligned}\left(\hbar\frac{\mathrm{d}}{\mathrm{d}t} + \kappa_\xi + \Gamma + i\left(\tilde{\varepsilon}_\nu^\mathrm{e} + \tilde{\varepsilon}_\nu^\mathrm{h} - \hbar\omega_\xi\right)\right)\langle b_\xi^\dagger v_\nu^\dagger c_\nu\rangle \\ = f_\nu^\mathrm{e} f_\nu^\mathrm{h} - \left(1 - f_\nu^\mathrm{e} - f_\nu^\mathrm{h}\right)\langle b_\xi^\dagger b_\xi\rangle \\ + i\left(1 - f_\nu^\mathrm{e} - f_\nu^\mathrm{h}\right)\sum_\alpha V_{\nu\alpha\nu\alpha}\langle b_\xi^\dagger v_\alpha^\dagger c_\alpha\rangle \\ + \sum_\alpha C^\mathrm{x}_{\alpha\nu\nu\alpha} + \delta\langle b_\xi^\dagger b_\xi c_\nu^\dagger c_\nu\rangle - \delta\langle b_\xi^\dagger b_\xi v_\nu^\dagger v_\nu\rangle\,. \quad (1.25)\end{aligned}$$

Here, the free evolution of $\langle b_\xi^\dagger v_\nu^\dagger c_\nu\rangle$ is determined by the detuning of the QD transitions from the optical modes. Hartree–Fock (singlet) contributions of the Coulomb interaction with the Coulomb matrix element $V_{\nu\alpha\nu\alpha}$ lead to the appearance of renormalized energies $\tilde{\varepsilon}_\nu^{\mathrm{e,h}}$ and to the interband exchange contribution that couples the photon-assisted polarizations from different states α. The source term of spontaneous emission is described by an expectation value of four carrier operators $\langle c_\alpha^\dagger v_\alpha v_\nu^\dagger c_\nu\rangle$. We have discussed the implications arising from this source term in Sect. 1.4. For uncorrelated carriers, the Hartree–Fock factorization of this source term leads to $f_\nu^\mathrm{e} f_\nu^\mathrm{h}$, which appears as the first term on the right-hand side of (1.25). Correlations remaining after the factorization are provided by the Coulomb and light-matter interaction between the carriers and are included in $C^\mathrm{x}_{\alpha'\nu\nu'\alpha} = \delta\langle c_{\alpha'}^\dagger v_\nu^\dagger c_{\nu'} v_\alpha\rangle$.

The stimulated emission/absorption term in the second line appears as the singlet-doublet factorization of the initial operator averages $\langle b_\xi^\dagger b_\xi c_\nu^\dagger c_\nu\rangle - \langle b_\xi^\dagger b_\xi v_\nu^\dagger v_\nu\rangle$. It is proportional to the photon number $\langle b_\xi^\dagger b_\xi\rangle$ in the mode ξ, thus providing feedback due to the photon population in the cavity. The correlations left after the factorization are given by the last two terms in (1.25). These are triplet-level carrier–photon correlations. These and higher order correlations are required for the calculation of the photon statistics in Sect. 1.5.2.

In (1.25) there are two terms acting as a dephasing: Photon dissipation κ_ξ and carrier–carrier and carrier–phonon interaction-induced dephasing. The latter is included via a phenomenological damping constant Γ in connection

with transition amplitudes $\propto v_\nu^\dagger c_\nu$. A more rigorous treatment of the dephasing in connection with the scattering rates can be provided by reservoir interaction via Lindblad terms, as discussed in Sect. 1.3.1. The most stringent approach would be the inclusion of the relevant physical processes, such as interaction with phonons, on a microscopic level.

After this general introduction to the theoretical model, we now formulate the laser equations for a coupled QD-microcavity system. We consider QDs with two localized shells for electrons and holes. The dots are embedded in a microcavity that provides one long-lived mode that is in resonance with the QD s-shell emission. Higher cavity modes are assumed to be energetically well separated from this mode, and a continuum of leaky modes and other cavity modes constitute the background of non-lasing modes.

In the following scheme, several assumptions are included, which are justified by possible experimental conditions and which lead to a convenient formulation of the theory. They provide no principle limitations and their use can be circumvented at the cost of more complicated analytical and numerical formulations. We assume that optical processes involving the laser mode (stimulated and spontaneous emission as well as photon reabsorption) are exclusively connected to the s-shell transitions. The carrier generation is assumed to take place in the p-shell, from which down-scattering into the s-shell is treated in a relaxation-time approximation. At the considered low temperatures of around 10 K, up-scattering processes are negligible. Carrier excitation in the WL or the barrier material, in which the QDs are embedded is often used in experiments. While it has the same effect as p-shell excitation for the laser dynamics from the QD s-shells, the density of states of the excited states strongly influences the effects of Pauli blocking.

When using QDs as the active material in microcavities, the coupling strength is determined by the position of the dots and their resonance frequencies. Inhomogeneous broadening is accounted for in the estimation of the number of QDs in resonance with the laser mode, but is not explicitly included in the equations of motion. The number of strongly coupled QDs can be estimated from the dot area density and the overlap of the cavity resonance with the inhomogeneously broadened ensemble of QDs. For the considered micropillar cavities with diameters of a few microns, a small number of tens of QDs can be considered to be in perfect resonance with the cavity mode.

Regarding the influence of the Coulomb interaction, we distinguish between the single-particle renormalizations and carrier correlations on the two-particle level. The renormalizations of the single-particle properties are indirectly included by assuming QDs on resonance with the cavity mode and a certain radiative lifetime in this mode, which is adapted from experiments. From previous calculations for the photoluminescence of QDs in microcavities [17] and emission from QDs in unstructured samples [22] we expect that the influence of carrier correlations on the stationary properties of the laser light emission is small. In current calculations we have therefore neglected these contributions.

Under the discussed conditions we now derive the equations for the semiconductor laser model. It is the greatest strength of our microscopic model that the accommodation of modifications is straightforward and follows a well-defined manner.

For the resonant s-shell/laser-mode transition, the equation of motion (1.25) for the photon-assisted polarization takes the form

$$\left(\hbar\frac{\mathrm{d}}{\mathrm{d}t} + \kappa + \Gamma\right)\langle b^\dagger v_s^\dagger c_s\rangle = f_s^\mathrm{e} f_s^\mathrm{h} - (1 - f_s^\mathrm{e} - f_s^\mathrm{h})\,\langle b^\dagger b\rangle + \delta\langle b^\dagger b c_s^\dagger c_s\rangle - \delta\langle b^\dagger b v_s^\dagger v_s\rangle, \tag{1.26}$$

where, from now on, the index $\xi = \xi_\mathrm{l}$ is omitted for the laser mode. In the equation of motion for the photon-assisted polarization of the non-lasing modes, the negligible photon population and the short lifetime of these modes allows for the omission of the feedback term and carrier–photon correlations,

$$\left(\hbar\frac{\mathrm{d}}{\mathrm{d}t} + \kappa_\xi + \Gamma + i\left(\varepsilon_s^\mathrm{e} + \varepsilon_s^\mathrm{h} - \hbar\omega_\xi\right)\right)\langle b_\xi^\dagger v_s^\dagger c_s\rangle\Big|_{\xi\neq\xi_\mathrm{l}} = f_s^\mathrm{e} f_s^\mathrm{h}. \tag{1.27}$$

As a result, (1.27) can be solved in the adiabatic limit and the part $\xi \neq \xi_\mathrm{l}$ of the sum in (1.24) can be evaluated, yielding a time constant τ_nl for the spontaneous emission into non-lasing modes in a fashion similar to the Weißkopf–Wigner theory [23],

$$\frac{2}{\hbar}\,\mathrm{Re}\sum_{\xi\neq\xi_\mathrm{l}}\frac{|g_\xi|^2}{\kappa_\xi + \Gamma + i\left(\varepsilon_s^\mathrm{e} + \varepsilon_s^\mathrm{h} - \hbar\omega_\xi\right)} = \frac{1}{\tau_\mathrm{nl}}\,. \tag{1.28}$$

In a laser theory, one typically distinguishes between the rate of spontaneous emission into lasing and non-lasing modes, $1/\tau_\mathrm{l}$ and $1/\tau_\mathrm{nl}$, respectively. Both rates add up to the total spontaneous emission rate $1/\tau_\mathrm{sp}$. Then the spontaneous emission factor is given by

$$\beta = \frac{\frac{1}{\tau_\mathrm{l}}}{\frac{1}{\tau_\mathrm{sp}}} = \frac{\frac{1}{\tau_\mathrm{l}}}{\frac{1}{\tau_\mathrm{l}} + \frac{1}{\tau_\mathrm{nl}}} \tag{1.29}$$

and the rate of spontaneous emission into non-lasing modes can be expressed according to

$$\frac{1}{\tau_\mathrm{nl}} = \frac{1-\beta}{\tau_\mathrm{sp}}. \tag{1.30}$$

From (1.24) one can now determine the population dynamics in the s-shell. For the spontaneous emission into non-lasing modes, the adiabatic solution of (1.27) is used according to (1.28) and (1.30). Furthermore, we include a transition rate of carriers from the p- to the s-shell in an approximation where only downwards directed scattering is considered, $R_{p\to s}^\mathrm{e,h} = (1 - f_s^\mathrm{e,h})\, f_p^\mathrm{e,h}/\tau_\mathrm{r}^\mathrm{e,h}$, and $g \equiv g_{\xi_\mathrm{l}}$ to obtain

$$\frac{\mathrm{d}}{\mathrm{d}t} f_s^{\mathrm{e,h}} = -\frac{2\,|g|^2}{\hbar}\mathrm{Re}\,\langle b^\dagger v_s^\dagger c_s\rangle - (1-\beta)\,\frac{f_s^{\mathrm{e}} f_s^{\mathrm{h}}}{\tau_{\mathrm{sp}}} + R_{p\to s}^{\mathrm{e,h}}. \tag{1.31}$$

Here the first term describes the carrier dynamics due to the interaction with the laser mode, while the second term represents the loss of carriers into non-lasing modes. The blocking factor $1-f_s^{\mathrm{e,h}}$ in $R_{p\to s}^{\mathrm{e,h}}$ ensures that the populations cannot exceed unity.

The carrier dynamics for the p-shell can be written as

$$\frac{\mathrm{d}}{\mathrm{d}t} f_p^{\mathrm{e,h}} = P\,(1-f_p^{\mathrm{e}}-f_p^{\mathrm{h}}) - \frac{f_p^e f_p^{\mathrm{h}}}{\tau_{\mathrm{sp}}^p} - R_{p\to s}^{\mathrm{e,h}}, \tag{1.32}$$

where a carrier generation rate P is included together with the Pauli-blocking factor $(1-f_p^{\mathrm{e}}-f_p^{\mathrm{h}})$. As the carrier generation takes place in the p-shell of each QD, P is to be understood as a "pump rate per emitter," in contrast to the pump rate $\tilde{P} = N_{\mathrm{emitter}}P$ appearing in (1.6). The second term describes spontaneous recombination of p-shell carriers and the third contribution is the above-discussed carrier relaxation.

Without the carrier–photon correlations $\delta\langle b_\xi^\dagger b_\xi c_\nu^\dagger c_\nu\rangle$ and $\delta\langle b_\xi^\dagger b_\xi v_\nu^\dagger v_\nu\rangle$, the resulting set of equations (1.31) and (1.32), together with (1.23) and (1.26) constitute the basic equations of the semiconductor laser model on the doublet level. They describe the coupled dynamics for the photon number and the carrier population.

1.5.2 Photon Statistics

To access intensity correlations, we must go beyond the doublet level and include all terms consistently up to the quadruplet level in the cluster expansion. Regarding these higher-order correlations, it is helpful to assume that only photons from the laser mode linger long enough to build up correlations.

The photon statistics follows from (1.22). The time evolution of the intensity correlation function $\delta\langle b^\dagger b^\dagger bb\rangle$ is given by

$$\left(\hbar\frac{\mathrm{d}}{\mathrm{d}t} + 4\kappa\right)\delta\langle b^\dagger b^\dagger bb\rangle = 4\,|g|^2\,\mathrm{Re}\sum_{\nu'}\delta\langle b^\dagger b^\dagger b v_{\nu'}^\dagger c_{\nu'}\rangle, \tag{1.33}$$

where the sum involves all resonant laser transitions from various QDs. In this equation enters another quadruplet function, which represents a correlation between the photon-assisted polarization and the photon number. For it and the two correlation functions in the last line of (1.26) more equations of motion must be solved, which we do not spell out here. Within reasonable approximations, the system of coupled equations now describing both the photon number and the second-order photon autocorrelation function closes on the quadruplet level.

From the derived equations, it is possible to obtain approximate analytic expressions for the second-order correlation function. Before the numerical

results of the semiconductor model are presented, it is instructive to study the two limiting cases of strong and weak pumping. Above the threshold the photon number becomes large, so that the limit $\langle b^\dagger b\rangle/N \gg 1$ can be fulfilled. In this case we obtain $g^{(2)}(0) = 1$, i.e., well above threshold the light is coherent. For the limiting case of weak pumping, stimulated emission and the higher-order correlations $\delta\langle b^\dagger b c_\nu^\dagger c_\nu\rangle$, $\delta\langle b^\dagger b v_\nu^\dagger v_\nu\rangle$ in (1.26) can be neglected due to the lack of a photon population. In the "bad cavity limit" [5], where the cavity loss rate is much larger than the total rate of spontaneous emission into the laser mode, we obtain

$$g^{(2)}(0) = 2 - \frac{2}{N}. \tag{1.34}$$

This is an important result, as it provides the statistics of thermal light in the limit of many QDs, $g^{(2)}(0) = 2$, and in the opposite limit of a single QD it gives the statistics of a single-photon emitter, $g^{(2)}(0) = 0$. The correlation properties and possible realizations of single-photon sources are the topic of Chap. 6.

1.5.3 Numerical Results

We now present numerical solutions of the extended semiconductor laser theory including carrier–photon correlations based on (1.23), (1.26), (1.31)–(1.33) and equations for higher-order correlations not explicitly given here. We consider a typical parameter set: The number of emitters is $\tilde{N} = 20$. The number used in the calculations is increased with decreasing β in order to have the thresholds occur at the same pump rate, i.e., $N = \tilde{N}/\beta$. For the spontaneous emission time enhanced by the Purcell effect we use $\tau_{\rm sp} = 50\,\text{ps}$, and the cavity damping is $\kappa = 20\,\mu\text{eV}$. The corresponding cavity lifetime is about 17 ps, yielding a Q-factor of roughly 30,000. The effective relaxation times for electrons and holes are taken to be $\tau_{\rm r}^{\rm e} = 1\,\text{ps}$ and $\tau_{\rm r}^{\rm h} = 500\,\text{fs}$, respectively.

In Fig. 1.8 the autocorrelation function $g^{(2)}(\tau = 0)$ is shown atop the input/output curve for various values of the spontaneous emission coupling β. There are several striking features:

1. The jump of the intensity curve from below to above threshold is no longer determined by $1/\beta$, like in Fig. 1.4 and many examples found in the literature [5, 24, 25] that are obtained from an atomic laser theory.
   The origin of the jump lies in the transition from dominantly spontaneous to stimulated emission in the system. As the non-lasing modes are only fed by spontaneous emission, their effect is that a fraction $1 - \beta$ of the total spontaneous emission is lost for the laser mode. Above the intermediate threshold region, stimulated emission into the laser mode dominates, so that losses into non-lasing modes are irrelevant. In the regime where spontaneous emission dominates, i.e., below the threshold, the output-power is reduced accordingly, visible as a jump in the input/output curve. In atomic systems operating at full inversion, like conventional four-level gas

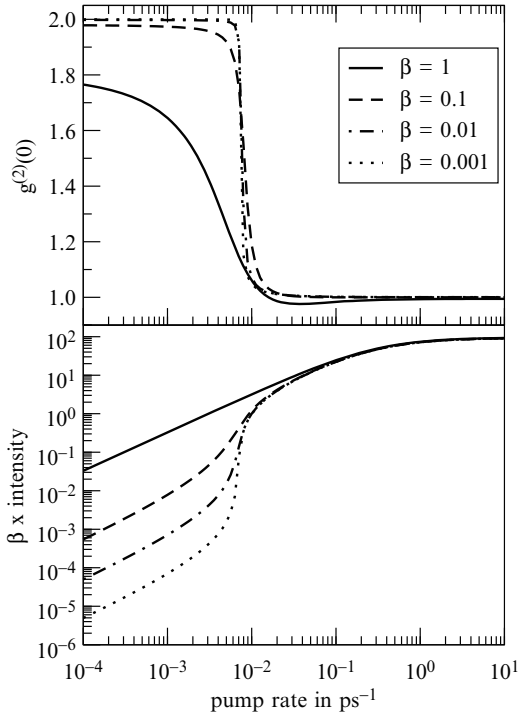

Fig. 1.8. Calculated input/output curve (*lower panel*) and autocorrelation function $g^{(2)}(\tau = 0)$ (*upper panel*) for $\beta = 1, 0.1, 0.01$, and 0.001. The system is excited at a constant pump rate, corresponding to continuous wave excitation

lasers, the height of the resulting jump is truly given by $1/\beta$. The fact that QD-based laser shows different behavior lies in the reabsorption present in the system, i.e., the laser does not operate at full inversion.
This is of particular importance since measurements of the input/output characteristics are often used to experimentally deduce the β-factor according to the predictions of the two-level models. If the atomic $1/\beta$-behavior would be used to extract the β-factors from the curves in Fig. 1.8, one would obtain 0.017 instead of 0.1, 0.0017 instead of 0.01, and 0.00017 instead of 0.001.

2. The usual laser threshold in conventional lasers with low spontaneous emission coupling ($\beta \sim 10^{-6}$) is very abrupt. We see that for larger β values ($\beta > 0.1$), the s-shaped jump in the input/output curve becomes smeared out, and also the drop of the autocorrelation function becomes softer.
3. For small β values, the intensity jump is accompanied by a decrease of the second-order coherence from the Poisson value $g^{(2)}(0) = 2$ for thermal light to $g^{(2)}(0) = 1$ for coherent laser light. For higher spontaneous emission coupling β, $g^{(2)}$ remains smaller than two below the

threshold. Corresponding to the discussion above, this behavior can arise either in the bad cavity regime if the number of emitters is small (compare (1.34)), or if the loss rate from the cavity becomes smaller than the rate of spontaneous emission into the cavity. In the latter case, and this is the reason for the decrease of sub-threshold value of $g^{(2)}(0)$ in Fig. 1.8, a substantial population of photons can build up in the cavity mainly due to spontaneous emission processes, and exhibit a deviation from the signature of incoherent thermal light. Furthermore, for the largest β value an antibunching signature is observed just above the threshold region, where $g^{(2)}(0)$ is smaller than 1.

4. At high pump intensities saturation effects due to Pauli blocking become visible in the input/output curve, effectively limiting the maximum output that can be achieved. The strength of the Pauli blocking depends on the number of available states in the pump levels and the number of QDs in resonance with the laser mode. When pumping into the barrier, where the density of states is larger than for the localized states, saturation effects will be less influential compared to the situation where higher localized states are pumped.

1.6 First-Order Coherence and Two-Time Quantities

Coherence is usually associated with the occurrence of fringes in an interference experiment. Chapter 6 gives details on experiments using a Michelson interferometer, where a quasi-monochromatic beam is divided into two by a beam splitter. By means of a moving mirror, a time delay τ is introduced to one of the beams before they are reunited. Only if this time delay is shorter than the coherence time τ_c, interference fringes can be observed between the two beams. The visibility of the interference fringes is directly described by the first-order correlation function, which we have written in terms of photon operators for the laser mode in (1.1). The loss of coherence carries over to the second-order correlation function $g^{(2)}(\tau)$. No matter if the light is thermal, coherent or exhibits an antibunching signature – the correlation function converges to a value of unity on a timescale of the coherence time. The coherence time can be calculated from the first-order correlation function:

$$\tau_c = \int_{-\infty}^{\infty} |g^{(1)}(\tau)|^2 \mathrm{d}\tau. \tag{1.35}$$

In quantum optics two-time operator averages, like (1.1), are accessed by invoking the quantum regression theorem [15, 26]. The quantum regression theorem in its standard formulation in quantum optics, however, requires the equations of motion to be linear and, therefore, applies to systems where only a single excitation is possible. Due to the unavoidable factorization of the equations of motion in the semiconductor model, the initial linearity of the model is spoiled. With the source-term of spontaneous emission, our equations

are nonlinear already on the singlet level, so that the validity of approaches that can be traced back to the quantum regression theorem rely on additional assumptions.

A straightforward approach for the calculation of $g^{(1)}(\tau)$ lies in the equation-of-motion-technique itself, where the time derivative is now taken with respect to the delay time τ [27]. In order to obtain the dynamics of a quantity $F(t, t+\tau)$ with respect to the time difference τ, in a first step the single-time problem is solved for $\tau = 0$. In a second step, the τ-evolution is evaluated according to its own equation of motion. The initial value is given by the $\tau = 0$ result obtained in the first step.

One has to be aware that for operators with different time arguments the commutation relations do not apply, i.e., $\langle b^\dagger(t)b^\dagger(t+\tau)b(t+\tau)b(t)\rangle \neq \langle b^\dagger(t)b^\dagger(t+\tau)b(t)b(t+\tau)\rangle$. Therefore, the number of equations in the resulting hierarchy that needs to be solved quickly scales with the order of the initial two-time expectation value. This method is now demonstrated in the calculation of the first-order coherence function. We use the Hamiltonian and the methods introduced in Sect. 1.5. In order to obtain non-rotating dynamical equations, we introduce

$$G(\tau) = e^{\mathrm{i}\omega\tau}\langle b^\dagger(t)b(t+\tau)\rangle. \tag{1.36}$$

The quantity defined in (1.36) obeys the following equation of motion

$$\left(\hbar\frac{\mathrm{d}}{\mathrm{d}\tau} + \kappa\right) G(\tau) = \sum_\nu g_\nu^* P_\nu(\tau), \tag{1.37}$$

where we have introduced the two-time photon-assisted polarization

$$P_\nu(\tau) = e^{\mathrm{i}\omega\tau}\langle b^\dagger(t)v_\nu^\dagger(t+\tau)c_\nu(t+\tau)\rangle. \tag{1.38}$$

We now invoke the same assumptions that we have used in the definition of the laser system in Sect. 1.5.1. In the following we consider N identical QDs that are on resonance with the laser mode. Furthermore, terms coupling different modes are neglected. With $g^{(1)}(\tau)$ being a doublet quantity (two-particle average) in the cluster expansion scheme, we truncate the hierarchy consistently at the same level. With these approximations, we finally arrive at the closed set of equations

$$\left(\hbar\frac{\mathrm{d}}{\mathrm{d}\tau} + \kappa\right) G(\tau) = g^* P(\tau), \tag{1.39}$$

$$\left(\hbar\frac{\mathrm{d}}{\mathrm{d}\tau} + \Gamma\right) P(\tau) = gN(f^c - f^v)G(\tau), \tag{1.40}$$

where we have introduced $P(\tau) = \sum_\nu P_\nu(\tau)$. The solution of these equations yields the normalized first-order correlation function

$$\left|g^{(1)}(\tau)\right| = \frac{-\gamma_-}{\gamma_+ - \gamma_-}e^{-\gamma_+|\tau|} + \frac{\gamma_+}{\gamma_+ - \gamma_-}e^{-\gamma_-|\tau|} \tag{1.41}$$

with

$$\hbar\gamma_{\pm} = \frac{\kappa + \Gamma}{2} \pm \sqrt{|g|^2 N(f^c - f^v) + \frac{(\kappa - \Gamma)^2}{4}} \,. \tag{1.42}$$

Thus, on the doublet level the first-order coherence properties are determined by the carrier populations in the lowest confined QD states, which are known from the stationary solutions of the dynamic laser equations. From (1.35) and the equations above, we find for the coherence time

$$\tau_{\mathrm{c}} = \frac{1}{\gamma_+} + \frac{1}{\gamma_-} + \frac{\hbar}{\kappa + \Gamma} \,. \tag{1.43}$$

In Fig. 1.9 the coherence times obtained from (1.42) and (1.43) are shown together with the input/output curves for three different values of the spontaneous emission coupling factor β. The parameters for the $\beta = 0.01$ curve are chosen to meet the characteristics of a real existing micropillar: $N = 500$ QDs, total spontaneous emission time $\tau_{\mathrm{sp}} = 80\,\mathrm{ps}$, homogeneous QD broadening

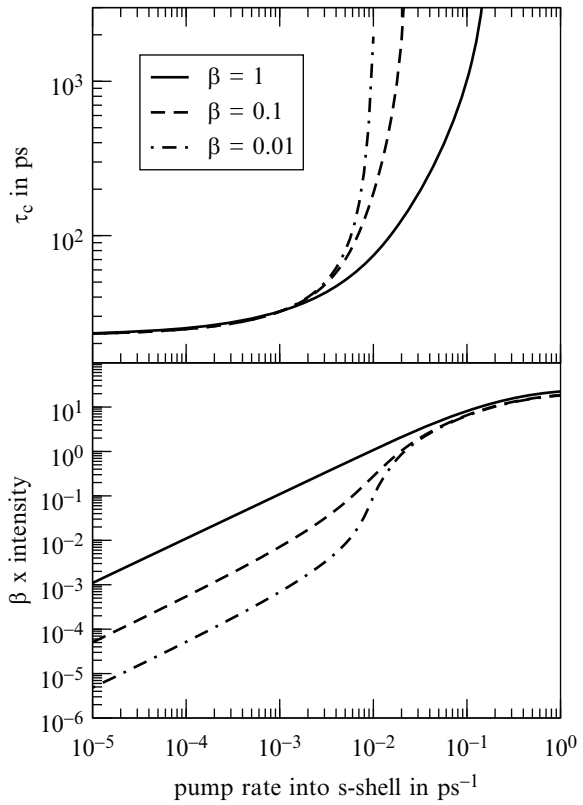

Fig. 1.9. Theoretical i/o curves (*bottom*) and coherence times (*top*) for various values of the β parameter. For $\beta = 0.01$, $\beta = 0.1$ and $\beta = 1{,}500$, 50 and 5 QDs have been used, respectively. All other parameters remain unaltered

$\Gamma \approx 200\,\mu\text{eV}$, and cavity losses $2\kappa = 30\,\mu\text{eV}$. For the $\beta = 0.1$ ($\beta = 1$) curve, $N = 50$ (5) QDs was used. As the threshold region is approached, a strong increase in the coherence time is observed. While below threshold the value lies between 20 and 30 ps for all three curves, the coherence time is found to increase slower with increasing pump power in cavities with larger spontaneous emission coupling: At comparable points on the input/output curves, we find that devices with a larger β factor display shorter coherence times. An illustrative explanation is that fluctuations introduced by spontaneous emission processes decrease the coherence in the system, and at higher β values more spontaneous emission is coupled into the laser mode. At the same time, even in the "thresholdless" case of $\beta = 1$, the slower, but nevertheless distinct rise in the coherence time indicates the beginning of the threshold region.

The decay of the first-order correlation function is presented in Fig. 1.10. A clear qualitative change of the decay from a Gaussian-like profile to a more exponential behavior can be observed within the transition regime. This qualitative change of the lineshape can be seen in the analytical solutions of the coherence function. Expanding (1.41) into a Taylor series reveals the Gaussian-like characteristic in the decay of $|g^{(1)}(\tau)|$, as the term linear in τ drops out. Considering the solutions $\gamma_{\pm}$ at transparency, $f^c - f^v = 0$, we get $\gamma_+ = \Gamma \gg \gamma_- = \kappa$, yielding a decay that is close to exponential $|g^{(1)}(\tau)| = e^{-\gamma_- \tau}$.

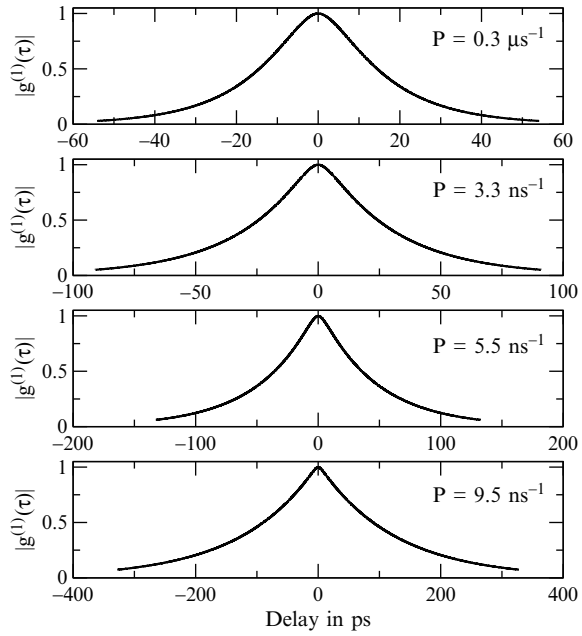

Fig. 1.10. Decay of the first-order correlation function at different excitation powers. A gradual change in the profile from Gaussian-like to a more exponential behavior becomes evident with increasing excitation power P

1.7 Concluding Remarks

We have reviewed the common methods in quantum optics for the computation of laser properties and placed them in relation to each other and to the equation-of-motion approach that our semiconductor theory is based on. As the most fundamental method we have discussed the Liouville/von-Neumann equation that yields the time-evolution of the full density matrix. This model can be reduced to a master equation that describes probabilities, or to the well-known rate equations. Two points are important to notice: Firstly, in both approaches where the density matrix elements are calculated, information about the statistical properties of the light are preserved, whereas in the rate equation formulation this information is lost. And secondly, we have discussed that the rate equations are the most simple possible factorization in a reformulation of the first two approaches in a hierarchy of coupled equations of motion.

In this context we place our semiconductor theory: It is based on an equation-of-motion approach. While rate equations typically describe the carrier system in terms of the expectation value of the number of excited two-level systems, the semiconductor approach is based on population expectation values and transition amplitudes in a semiconductor basis. Also the hierarchy of equations is not truncated on the semiclassical level, but higher-order correlation functions are kept in a consistent manner. This enables us to calculate the coherence properties of the emitted light in terms of the second-order correlation function. As the equation-of-motion method does not require the equations to be linear, Coulomb correlations and other effects specifically important in semiconductor systems can be included in a straightforward way. To give an illustrative example for a deviation from the atomic behavior, we have discussed the source term of the spontaneous emission, which is modified due to the possibility to have more than single excitation in a QD. As a consequence, the carrier decay and the photoluminescence exhibits a non-exponential signature with a density-dependent decay rate. This effect is naturally included in our semiconductor approach. While it is possible to modify existing quantum-optical models to include more than a single excitation per emitter, it has, to the best of our knowledge, not been done so far. In this sense, our approach can be understood as an extension to these models. However, being based on a microscopic Hamiltonian, the full spectrum of semiconductor effects, including Coulomb effects and interaction with phonons, can be considered on a microscopic level.

In order to calculate the first-order coherence properties we have shown how the described model can be used to calculate two-time operator averages. With this and the second-order correlation function, we obtain a consistent overall picture of the laser transition in QD-based microcavity laser devices. At the large spontaneous emission coupling factors β that are currently obtained in state-of-the-art devices, the transition in the input/output characteristics is washed-out and cannot be clearly identified anymore. At the same time,

around the threshold region we observe a distinct rise in the coherence time by about two orders of magnitude, a change in the lineshape of the first-order correlation function from Gaussian-like to exponential, and a change in the second-order coherence properties from (close to) the signature of thermal light ($g^{(2)}(0) = 2$) to that of coherent ($g^{(2)}(0) = 1$) light. These results characterize clearly the physics in the threshold region even if a threshold is no longer directly visible in the intensity of the emitted light.

From atomic models it is expected that the output intensity shows a jump by a factor of $1/\beta$ at the threshold. For several reasons this does not apply to semiconductor systems. The reabsorption present in the system modifies the height of the jump. Saturation effects of the pump levels and due to the small numbers of QDs typically present in microcavity lasers, can have an effect at higher excitation powers. In this case the upper branch of the input/output curve can be masked to an extent where even the threshold is not fully developed. If in this case atomic models are used to extract parameters from measured data, the smaller jump in the input/output characteristics may be mistaken to be caused by a spontaneous emission coupling factor β larger than it truly is. This effect is even more pronounced for pulsed excitation [28].

The close relation to the discussed atomic models allows for a direct comparison and a verification of the truncation scheme if the semiconductor model is considered in the limit of a single possible excitation. We have performed such tests for an ensemble of emitters and find that the truncation of the hierarchy introduced by the light-matter coupling on the quadruplet level delivers an accurate description of the laser properties including the second-order correlation function for realistic parameters [19].

Acknowledgments

In the end we would like to thank our colleagues in the experimental groups in Stuttgart (S. Ates, S.M. Ulrich, P. Michler) and Dortmund (T. Auer, T. Berstermann, M. Aßmann, M. Bayer), as well as Paul Gartner, Michael Lorke and Sandra Ritter in our own group for stimulating discussions and fruitful collaboration. Financial support from the DFG research group "Quantum optics in semiconductor nanostructures" and a grant for CPU time at the Forschungszentrum Jülich (Germany) is gratefully acknowledged.

References

1. E.M. Purcell, H.C. Torrey, R.V. Pound, Phys. Rev. **69**, 37 (1946)
2. P. Lodahl, A. Floris van Driel, I.S. Nikolaev, A. Irman, K. Overgaag, D. Vanmaekelbergh, W.L. Vos, Nature **430**, 654 (2004)
3. K.J. Vahala, Nature **424**, 839 (2003)
4. F. DeMartini, G.R. Jacobovitz, Phys. Rev. Lett. **60**, 1711 (1988)
5. P.R. Rice, H.J. Carmichael, Phys. Rev. A **50**, 4318 (1994). http://prola.aps.org/abstract/PRA/v50/p4318

6. G.S. Solomon, M. Pelton, Y. Yamamoto, Phys. Rev. Lett. **86**, 3903 (2001)
7. H.G. Park, S.H. Kim, S.H. Kwon, Y.G. Ju, J.K. Yang, J.H. Baek, S.B. Kim, Y.H. Lee, Science **305**, 1444 (2004)
8. S. Strauf, K. Hennessy, M.T. Rakher, Y.S. Choi, A. Badolato, L.C. Andreani, E.L. Hu, P.M. Petroff, D. Bouwmeester, Phys. Rev. Lett. **96**, 127404 (2006)
9. Y.S. Choi, M.T. Rakher, K. Hennessy, S. Strauf, A. Badolato, P.M. Petroff, D. Bouwmeester, E.L. Hu, Appl. Phys. Lett. **91**, 031108 (2007)
10. S.M. Ulrich, C. Gies, S. Ates, J. Wiersig, S. Reitzenstein, C. Hofmann, A. Löffler, A. Forchel, F. Jahnke, P. Michler, Phys. Rev. Lett. **98**, 043906 (2007)
11. R.J. Glauber, Phys. Rev. **130**, 2529 (1963)
12. T.R. Nielsen, P. Gartner, F. Jahnke, Phys. Rev. B **69**, 235314 (2004)
13. J. Seebeck, T.R. Nielsen, P. Gartner, F. Jahnke, Phys. Rev. B **71**, 125327 (2005)
14. Y. Mu, C.M. Savage, Phys. Rev. A **46**, 5944 (1992)
15. H.J. Carmichael, *Statistical Methods in Quantum Optics 1* (Springer, Berlin Heidelberg New York, 1999)
16. H. Yokoyama, S.D. Brorson, J. Appl. Phys. **66**, 4801 (1989)
17. M. Schwab, H. Kurtze, T. Auer, T. Berstermann, M. Bayer, J. Wiersig, N. Baer, C. Gies, F. Jahnke, J.P. Reithmaier, A. Forchel, M. Benyoucef, P. Michler, Phys. Rev. B **74**, 045323 (2006)
18. T. Berstermann, T. Auer, H. Kurtze, M. Schwab, M. Bayer, J. Wiersig, C. Gies, F. Jahnke, D. Reuter, A. Wieck, Phys. Rev. B **76**, 165318 (2007)
19. C. Gies, J. Wiersig, M. Lorke, F. Jahnke, Phys. Rev. A **75**, 013803 (2007)
20. J. Fricke, Ann. Phys. **252**, 479 (1996)
21. G. Khitrova, H.M. Gibbs, F. Jahnke, M. Kira, S.W. Koch, Rev. Mod. Phys. **71**, 1591 (1999)
22. N. Baer, C. Gies, J. Wiersig, F. Jahnke, Eur. Phys. J. B **50**, 411 (2006)
23. P. Meystre, M. Sargent III, *Elements of Quantum Optics* (Springer, Berlin, 1999)
24. G. Björk, Y. Yamamoto, IEEE Journal of Quant. Electr. **27**, 2386 (1991)
25. Y. Yamamoto, S. Machida, G. Björk, Phys. Rev. A **44**, 657 (1991)
26. Y. Yamamoto, A. Imamoğlu, *Mesoscopic Quantum Optics* (John Wiley & Sons, Inc., 1999)
27. S. Ates, C. Gies, S.M. Ulrich, J. Wiersig, S. Reitzenstein, A. Löffler, A. Forchel, F. Jahnke, P. Michler, Phys. Rev. B **78**, 155319 (2008)
28. C. Gies, J. Wiersig, F. Jahnke, Phys. Rev. Lett. **101**, 067401 (2008)

http://www.springer.com/978-3-540-87445-4

Single Semiconductor Quantum Dots
Michler, P. (Ed.)
2009, XVI, 390 p. 190 illus., 52 illus. in color., Hardcover
ISBN: 978-3-540-87445-4